

Hyperpolarized Gas Imaging in Lung Diseases: Functional and Artificial Intelligence Perspective

Ziwei Zhang¹, Haidong Li¹, Sa Xiao, Qian Zhou, Shiyuan Liu, Xin Zhou, Li Fan

Pathophysiologic changes in lung diseases are often accompanied by changes in ventilation and gas exchange. Comprehensive evaluation of lung function cannot be obtained through chest X-ray and computed tomography. Proton-based lung MRI is particularly challenging due to low proton density within the lung tissue. In this review, we discuss an emerging technology—hyperpolarized gas MRI with inhaled ¹²⁹Xe, which provides functional and microstructural information and has the potential as a clinical tool for detecting the early stage and progression of certain lung diseases. We review the hyperpolarized ¹²⁹Xe MRI studies in patients with a range of pulmonary diseases, including chronic obstructive pulmonary disease, asthma, cystic fibrosis, pulmonary hypertension, radiation-induced lung injury and interstitial lung disease, and the applications of artificial intelligence were reviewed as well.

Key Words: Hyperpolarized gas imaging; Xenon-129; Lung diseases; Magnetic resonance imaging; Artificial intelligence.

© 2024 The Association of University Radiologists. Published by Elsevier Inc. All rights reserved.

Abbreviation: **ADC** apparent diffusion coefficient, **AI** artificial intelligence, **CF** cystic fibrosis, **COVID-19** coronavirus disease 2019, **COPD** chronic obstructive pulmonary disease, **CT** computed tomography, **CSSR** chemical shift saturation recovery, **CS** compressed sensing, **DC-RDN** deep cascade of residual dense network, **DL** deep learning, **DL_{co}** diffusing capacity of the lungs for carbon monoxide, **DCE-MRI** dynamic contrast-enhanced magnetic resonance imaging, **DXeV-MRI** dynamic hyperpolarized ¹²⁹Xe ventilation MRI, **DW-MRI** diffusion-weighted MRI, **FRC** functional residual capacity, **FVC** forced vital capacity, **FEV₁** forced expiratory volume in 1 s, **FLASH** fast low angle shot, **HRCT** high resolution computed tomography, **IPF** idiopathic pulmonary fibrosis, **HP** hyperpolarized, **IVIM** intravoxel incoherent motion, **LCI** lung clearance index, **MRI** magnetic resonance imaging, **NSCLC** non-small cell lung cancer, **NMPA** national medical products administration, **TP** tissue and blood plasma, **PREFUL MRI** phase resolved functional lung MRI, **PEX** pulmonary exacerbation, **PH** pulmonary hypertension, **PFT** pulmonary function test, **PACS** post-acute COVID-19 syndrome, **PASC** post-acute sequelae of COVID-19, **QCT** quantitative computed tomography, **RBC** red blood cell, **SEOP** spin exchange optical pumping, **SARS-CoV-2** severe acute respiratory syndrome coronavirus 2, **SGRQ** St George Respiratory Questionnaire, **UTE** ultra-short echo time, **V/Q-SPECT** ventilation/perfusion single photon emission computed tomography, **VDP** ventilation defect percentage, **VCS** variable-sampling-ratio compressed sensing, **ZTE** zero echo time

INTRODUCTION

Due to air pollution, tobacco smoking, aging, and many other factors, lung diseases such as chronic obstructive pulmonary disease (COPD), asthma,

and idiopathic pulmonary fibrosis (IPF) are increasing (1), smoking has directly resulted in 80% of COPD deaths (2). Therefore, early diagnosis and treatment of lung diseases is a key issue. The most common imaging methods for the respiratory system are chest radiography and computed tomography (CT), which can provide diagnostic information on lung morphology such as emphysema and bronchodilation (3), but still can be restricted in clinical applications because of ionizing radiation and indirect evaluation of pulmonary function. Ventilation/perfusion single photon emission computed tomography (V/Q-SPECT) can provide quantitative information on ventilation and perfusion, but the temporal and spatial resolution is poor (4). Magnetic resonance imaging (MRI) is non-radiative with good soft tissue contrast and high sensitivity to changes in functional, hemodynamic, and other parameters (5).

However, the clinical application of conventional MRI is hindered due to the characteristic of extremely low signal in the lungs. Therefore, researchers have conducted a series of

Acad Radiol xxxx; xx:xxx-xxx

From the Department of Radiology, Second Affiliated Hospital of Naval Medical University, Shanghai 200003, People's Republic of China (Z.Z., S.L., L.F.); State Key Laboratory of Magnetic Resonance and Atomic and Molecular Physics, National Center for Magnetic Resonance in Wuhan, Wuhan Institute of Physics and Mathematics, Innovative Academy for Precision Measurement Science and Technology, Chinese Academy of Sciences-Wuhan National Laboratory for Optoelectronics, Huazhong University of Science and Technology, Wuhan 430071, China (H.L., S.X., Q.Z., X.Z.); University of Chinese Academy of Sciences, Beijing 100049, China (H.L., S.X., X.Z.). Received December 5, 2023; revised January 3, 2024; accepted January 8, 2024. **Address correspondence to:** L.F. e-mail: fanli0930@163.com

¹ These authors contributed equally to this work.

© 2024 The Association of University Radiologists. Published by Elsevier Inc. All rights reserved.

<https://doi.org/10.1016/j.acra.2024.01.014>

studies on the application of MRI to lung parenchyma with sequential imaging, such as intravoxel incoherent motion (IVIM) that show potentially powerful ability in the differential diagnosis of lung tumors (6), dynamic contrast-enhanced MRI that exhibit relatively high sensitivity for lung parenchymal lesions (7), and the emerging ultra-short echo time (UTE) MRI (8,9) and zero echo time (ZTE) MRI (10,11), that have great potential in the presentation of hyperventilation, emphysema, cysts, or bronchial lesions. Still, the pulmonary function cannot be directly evaluated and quantified with these above-mentioned imaging methods.

Lung MR imaging of hyperpolarised gases including helium-3 (^3He) and xenon-129 (^{129}Xe) (12,13), as inhaled MRI contrast agents offer information about both the function and microstructure of the lung and have potential as a clinical tool for detecting early-stage and progression of certain lung disease. Hyperpolarized ^3He MRI imaging has been reported that it can make a good analysis of the ventilation and tissue structure damage in COPD (14,15), asthma (16,17), cystic fibrosis (18,19) and radiation-induced lung injury (20). However, the disadvantage of ^3He is the limited and unpredictable global quantities and high cost, whereas ^{129}Xe has more gas inventory in nature and is more feasible for clinical studies. Moreover, Kirby et al (21) pointed out that the ventilation defect percentage (VDP) obtained with hyperpolarized ^{129}Xe MRI is significantly higher than that obtained with hyperpolarized ^3He MRI, and Peiffer et al indicated that hyperpolarized ^{129}Xe MRI can provide equivalent information to SPECT and spirometry measures in the latest article (22), hence it is reasonable to assume that hyperpolarized ^{129}Xe MRI has great potential for structural and functional abnormalities in lung disease.

In this review, we briefly illustrate HP ^{129}Xe MRI methodology, including principles and procedure, and what aspects of lung function (ventilation and gas exchange) they probe. In addition, we review the hyperpolarized gas MRI studies in patients with a range of pulmonary diseases, including COPD, asthma, cystic fibrosis, pulmonary hypertension, radiation-induced lung injury and interstitial lung disease, and the applications of artificial intelligence were reviewed as well.

HP GAS MRI PRINCIPLES AND PROCEDURES

Hyperpolarization technology is a method that can effectively improve the sensitivity of nuclear magnetic resonance, which can push the nuclear spin state to a state deviating from the thermodynamic equilibrium through physical or chemical processes, the intensity of the nuclear magnetic resonance signal is enhanced by several orders of magnitude and the magnetization vector is increased in this way (23). Spin exchange optical pumping (SEOP) is the widely used hyperpolarized technique that could enhance the polarization of noble gases by a factor of > 10000 (24,25).

The extremely high MR signal of hyperpolarised gas is "non-renewable" and could not recover by relaxation,

making the pulse sequence designs different from those used in conventional magnetic resonance imaging. Rapid acquisition with small flip angles is a simple method, and the pulse sequence based on the fast low-angle shot (FLASH) is widely used, although more sophisticated sequences such as b-SSFP which utilizes large flip angles are exploited for ultra-fast imaging (26). For the flip angle calibration of the RF pulse, the strategy that repeated acquisition with a small flip was generally used (27). Meanwhile, the T_1 measurement also utilized a similar strategy for the chemical shift calibration, the chemical shift of ^{129}Xe in the airspaces was generally set to 0 ppm, and then the chemical shifts of ^{129}Xe in the other components could be measured.

First, in the ^{129}Xe preparation and delivery section, the ^{129}Xe gas is hyperpolarized using a commercially available polarizer. Dosing volumes typically range from 500–1000 mL, which is a gas mixture of helium-4 and xenon-129, these hyperpolarised gases can be delivered to the subject via a Tedlar bag. The subject should inhale the gas mixture at the functional residual capacity (FRC). Second, in the image acquisition section, ^{129}Xe MRI is performed using different sequences based on the study requirement, such as FLASH, diffusion-weighted imaging (DWI), and chemical shift saturation recovery (CSSR). For the post-processed techniques, the quantitative indices analysis was performed with software or algorithm generated in Matlab.

Static Ventilation Imaging

^{129}Xe has a gaseous and dissolved phase after inhaling by the subject, direct MR imaging of gaseous ^{129}Xe by using the sequences of FLASH or UTE allows the visualization of the gas distribution and manifestation of the lung ventilation. Ventilation imaging includes static ventilation imaging and dynamic ventilation imaging. Static ventilation imaging is when a patient inhales ^{129}Xe and holds the breath for a while to obtain the image of the gas. The most common biomarker of static ventilation imaging is VDP, which can provide a relatively objective method to display ventilation distribution even in subjects who have pulmonary function impairment and is not applicable for spirometry (28) and has a prediction for outcomes in asthma (29).

Dynamic Ventilation Imaging

The standard way to do ventilation imaging is to collect static images during a breath hold, neglecting the possibility of delayed ventilation based on collateral ventilation (30) and the inaccuracy of VDP. To reduce the acquisition time, accelerated methods have been used, such as spiral encoding (31), compressed sensing (CS) and deep learning (DL) (32), for instance, Ajraoui et al pioneered the use of the CS algorithm for accelerating pulmonary hyperpolarized gas MRI (33), and Xiao et al refined the use of CS to achieve both high temporal and spatial resolution in pulmonary dynamic hyperpolarized gas MRI (34,35), as shown in Figure 1.

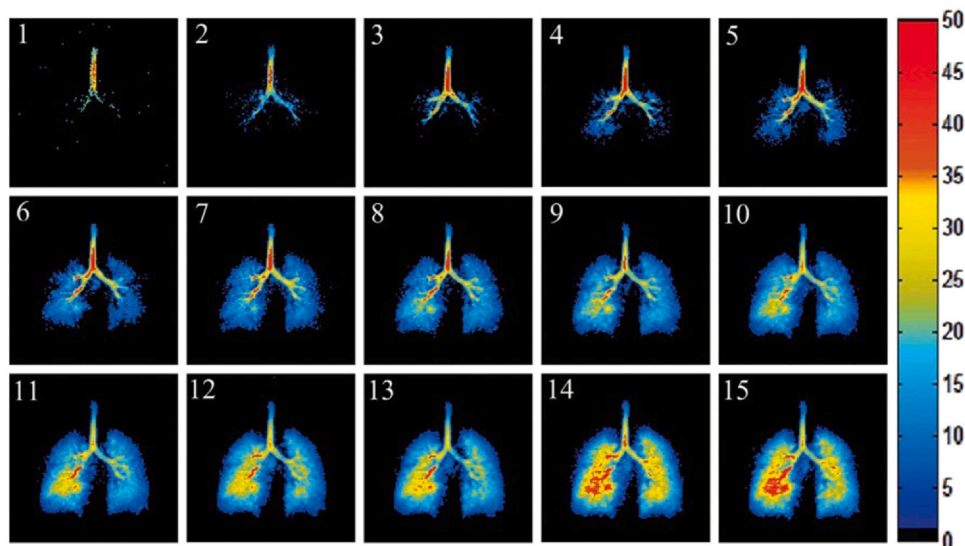


Figure 1. Dynamic visualization of the pulmonary ventilation process by hyperpolarized ^{129}Xe MRI (35).

Diffusion-weighted Imaging

Diffusion-weighted imaging with multiple b values is generally used for the microstructure of the lung assessment. The cylinder model and stretched-exponential model are the

theoretical models of hyperpolarized gas DWI signal (36), by which the morphological parameters could be obtained. However, the long acquisition time (> 15 s) is a big challenge for the clinical applications of ^{129}Xe DWI. More efforts have been made to accelerate the acquisition (37), for example,

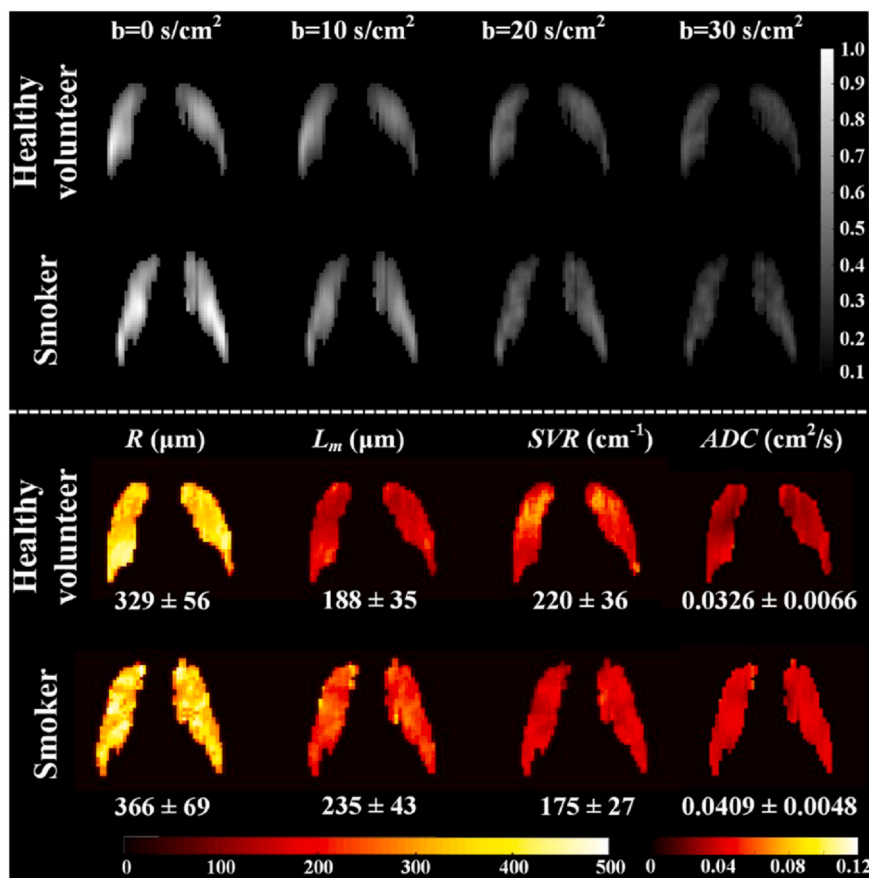


Figure 2. Lung images and morphometric parameter maps obtained from hyperpolarized ^{129}Xe VCS DWI for a healthy subject and a smoker (38).

the acquisition could be accelerated by 4 times without sacrificing the quality of the images when using variable-sampling-ratio compressed sensing (VCS) patterns (38), as shown in Figure 2. HP ^{129}Xe has been used to assess alveolar enlargement, however, some factors may impact the precision and accuracy of apparent diffusion coefficient (ADC) measurements, Bdaiwi et al suggested that HP ^{129}Xe diffusion MRI can be optimized by minimizing the uncertainty of ADC measurements through an analytical model (39). Moreover, Thomen et al tried to validate hyperpolarized Xenon as a biomarker for alveolar enlargement (40). Diffusion-weighted imaging has been used for a range of lung diseases, such as coronavirus disease 2019 (COVID-19) (41), cystic fibrosis (42) and emphysema (43).

Dissolved-phase Imaging

Dissolved ^{129}Xe exhibits distinct chemical shifts in lung tissue and blood plasma (TP) and red blood cell (RBC), allowing the function of gas exchange to be measured with spectroscopic imaging methods like chemical shift saturation recovery (CSSR). CSSR is the widely used method for measuring the gas exchange of ^{129}Xe between the alveolar space and lung tissue (44), and comprehensive physiological parameters could be obtained by using the gas exchange models like MOXE (45) and Patz (46). However, conventional phase-encoded chemical shift imaging has prevented clinically available tools due to long acquisition times. The one-point Dixon technique has been the most used method in studies of lung disease, for example, Kaushik et al suggested the feasibility of acquiring images of alveolar space, TP and RBC (47), and Niedbalski et al achieved the reduction of breath hold duration with the use of it (48). More advanced multi-point techniques were developed due to the certain limitations of the one-point Dixon method. A three-point IDEAL 3D radial implementation has been applied in subjects with COPD and asthma (49), and Kammerman et al (50) and Collier et al (51) proposed four-point spectroscopic imaging techniques in the populations of IPF. In a word, the development of multipoint methods not only improved the quality of images but also provided additional information. Generally, microstructure and gas exchange of the lung are assessed in separated breathholds. To reduce the cost of ^{129}Xe imaging in clinical applications, Xie and colleagues have successfully collected the DWI and dynamic spectroscopies within a single breath-hold (52).

THE APPLICATIONS OF HP ^{129}Xe MRI IN DIFFERENT LUNG DISEASES

Chronic Obstructive Pulmonary Disease

Chronic obstructive pulmonary disease (COPD) is the fourth leading cause of death in the world and the most common chronic terminal respiratory airway disease, which is characterized by chronic inflammatory reactions in the airways,

the repeated stimulation of inflammation leads to the presentation of ventilation dysfunction, decreased barrier (also called TP) uptake and RBC transfer in COPD patients (53). X-ray radiography and CT examinations have limited diagnostic value for COPD patients, pulmonary function tests (PFTs) are valuable in assessing and predicting the occurrence and progression of COPD in the clinical practice, as well as quantitatively assessing the respiratory physiology of COPD, but with some limitations in displaying specific focal lesion. In the diagnosis of COPD, additional information about the gas-exchange function of alveolar capillaries and RBC can be obtained through HP ^{129}Xe MRI (54).

To detect and quantify the delayed ventilation in COPD patients, 15 COPD patients underwent fast dynamic hyperpolarized ^{129}Xe ventilation MRI (DXeV-MRI), quantitative computed tomography (QCT) and spirometry tests. Delayed ventilation was demonstrated in 13 of the 15 COPD patients while no delayed ventilation was observed in the healthy group in DXeV-MRI images, but delayed ventilation was not observed in QCT and spirometry. Then Chen et al concluded that temporal ventilation was consistent with the expected physiological changes across a free-breathing cycle (55). In a study of lobar analysis conducted by Matin et al (56), HP ^{129}Xe MRI, QCT and spirometry tests were performed and percentage ventilated volume and ADC were obtained in 22 COPD patients, the presence of VDP differ in healthy group and COPD (as shown in Fig 3), and the results indicated that percentage ventilated volume and ADC values share a correlation with percentage emphysema at QCT and PFT results.

In another study exploring the changes in lung physiology (morphology and function), pulmonary function tests, chest CT, perfusion MRI, and HP ^{129}Xe MRI were performed in 4 COPD patients, several quantitative indexes reflecting the changes in lung physiology could be obtained in the study, such as tissue density with chest CT, pulmonary perfusion with perfusion MRI, and ventilation and gas exchange in HP ^{129}Xe MRI. These three imaging methods mentioned above were able to differentiate COPD patients from healthy volunteers according to the reported results, and Qing et al further noted that HP ^{129}Xe MRI can provide additional diagnostic information (57), such as focal airflow limitation, or underlying gas exchange impairment that does not appear to be a decrease in ventilation or perfusion.

In order to assess lobar ventilation in COPD patients, Doganay et al conducted a prospective study involving multiple imaging methods (58), in which rapid time-series HP ^{129}Xe MRI, V/Q-SPECT, high-resolution computed tomography (HRCT) and spirometry were implemented in the 12 COPD patients. The results showed lobar ventilation obtained with HP ^{129}Xe MRI strongly correlated with lobar ventilation and perfusion measurements derived from SPECT/CT, the correlation between the absolute CT percentage emphysema with CT and percentage ventilation with HP ^{129}Xe MRI was also statistically significant, which indicated that the feasibility of HP ^{129}Xe MRI in providing additional information in COPD.

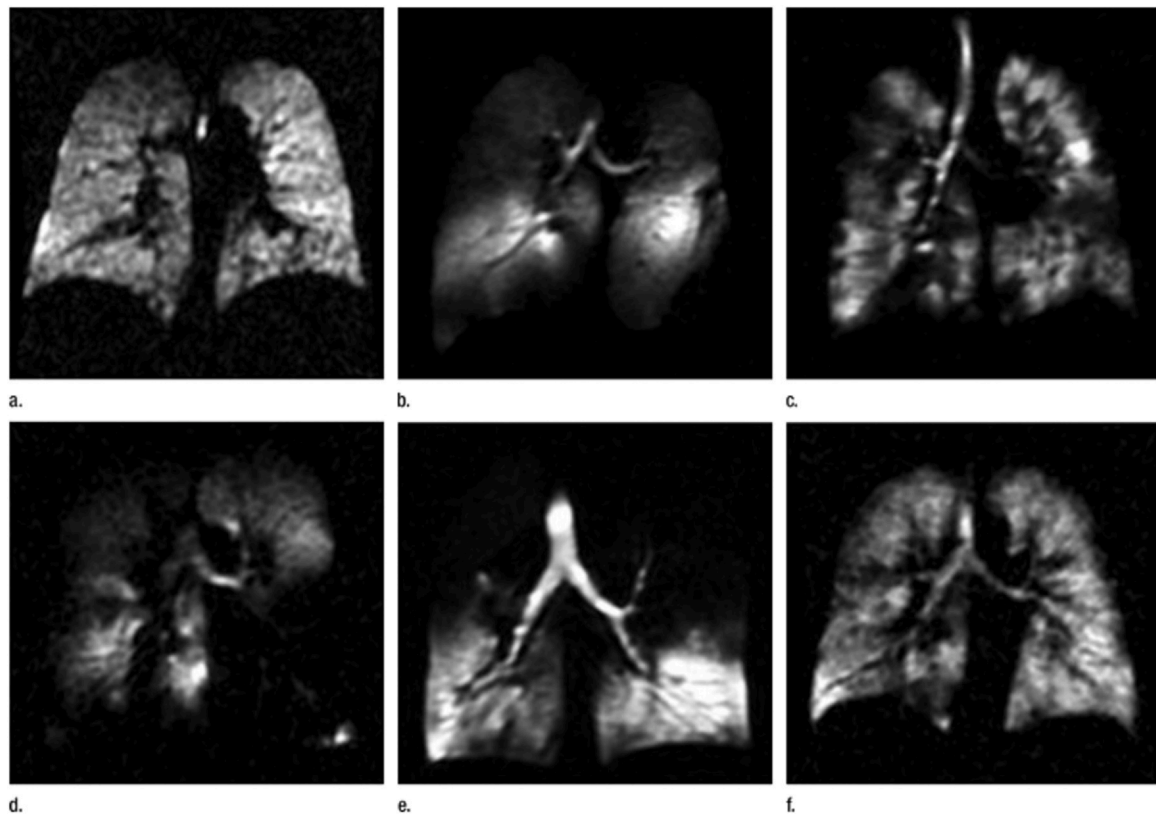


Figure 3. Representative ^{129}Xe ventilation slices of healthy volunteers (a) and COPD subjects (b-f) (56).

Idiopathic Pulmonary Fibrosis

Idiopathic pulmonary fibrosis (IPF) is a progressive interstitial lung fibrosis disease of unknown etiology, which is often characterized by varying degrees of structural and functional changes in the lungs (59). Pulmonary functional tests, including forced vital capacity (FVC) and diffusing capacity of the lungs for carbon monoxide (DL_{CO}), can quantify the degree of the strictness of IPF (60) but are relatively insensitive to the early stages of the disease. HRCT is a reliable diagnostic imaging tool for the diagnosis of IPF in clinical practice (61), however, there are still some limitations,

lesions detected on CT cannot be well correlated with the patient's clinical manifestation (62), in particular, progression and therapeutic response of disease cannot be well illustrated from the microstructural level such as alveoli and TP (63). The three-dimensional spatial measurement of lung structure and function (including barrier uptake and RBC transfer) can be realized in HP ^{129}Xe MRI. Furthermore, the RBC: barrier ratio is the most powerful indicator of gas exchange function impairment in current according to the range of pre-clinical studies (47,64). A sample image of gas exchange is shown in Figure 4, providing the ratios of barrier and gas, RBC and gas, and RBC and barrier.

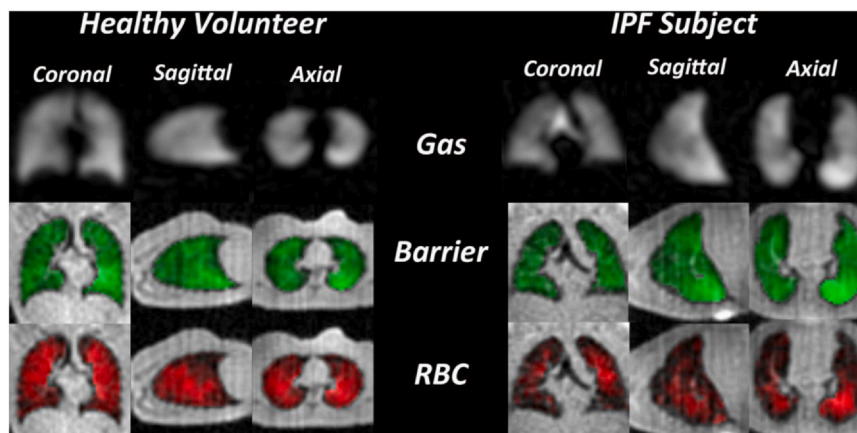


Figure 4. Ratios of the ^{129}Xe -barrier:gas, ^{129}Xe -RBC:gas, and the RBC:barrier images (63).

In a study of HP ^{129}Xe gas-transfer spectroscopy in patients with idiopathic pulmonary fibrosis, Kaushik first noted that the ratio of RBC to barrier was significantly decreased in IPF patients compared to healthy volunteers, and was strongly correlated with DL_{co} (64). Wang et al also quantified regional gas transfer in IPF patients using HP ^{129}Xe MRI (65), in this study, 12 IPF patients and 13 healthy volunteers both underwent HP ^{129}Xe MRI, 3D quantitative maps of ventilation, barrier uptake and RBC transfer were generated respectively, the results showed that ventilation was not significantly different from healthy volunteers in moderate IPF patients, while the barrier signal was significantly enhanced throughout the whole lung (206% of reference), more common located in subpleural regions, which accompanied by reduced RBC transfer (57% of reference). In the meantime, ventilation was decreased in severe IPF patients compared to healthy volunteers (83% of reference), with a highly elevated barrier uptake throughout most of the lung (200% of reference) and a reduced RBC transfer (49% of reference). In addition, the MRI metrics (ventilation, barrier uptake, RBC transfer, RBC: barrier ratio) were significantly correlated with PFT (FVC, DL_{co}), ventilation correlated moderately and positively with FVC but not significantly with DL_{co} , barrier uptake correlated significantly and negatively with FVC and DL_{co} , RBC transfer correlated significantly and positively with FVC and DL_{co} . However, the CT fibrosis score was weakly and insignificantly correlated with all MRI metrics, the results above indicated that HRCT can be used as a diagnostic basis for IPF, but may be relatively insensitive to underlying pulmonary fibrous disease.

Wang et al also determined that barrier tissue uptake was strikingly enhanced in IPF patients (54), most patients exhibited higher uptake in the lung periphery which was accompanied by reduced RBC transfer and focal defects (primarily located in the basal and periphery region), these defects regions that may be taken for a marker of diminished perfusion (64). The finding that significantly increased barrier uptake was accompanied by normal or elevated RBC transfer in some areas was noted as well, it may represent an early stage of the disease or a post-treatment response. Quantitative barrier ^{129}Xe uptake maps can reveal microstructural abnormalities in the lung, such as septal thickening and gas exchange surface area.

Hahn et al evaluated the progression of IPF using HP ^{129}Xe MRI (66), 22 IPF patients and 16 healthy volunteers were recruited, all participants underwent HP ^{129}Xe MRI and participants with IPF were followed up with PFTs (FEV and DL_{co}) at 1 year. In this study, the progression of IPF was defined as a reduction of at least 10% in FVC and 15% in DL_{co} , in the meantime, fibrotic and normal-appearing regions were classified on CT image. The results showed that there were 9 IPF progressors and 13 nonprogressors after a year, and there was a reduction of FVC and DL_{co} in IPF patients, furthermore, IPF progressors had reduced RBC: barrier ratio in the structurally normal-appearing lung at CT,

while RBC: barrier ratio appeared normal in fibrotic regions, which indicated that HP ^{129}Xe MRI may detect the progression of IPF and earlier than conventional imaging methods, especially when some regions appear normal on CT while lung function may already change.

A study involving healthy volunteer and IPF patients was conducted by Collier et al (51), for the quantification of regional gas transfer using dissolved ^{129}Xe lung MRI, reduced regional gas transfer was observed, and RBC/TP and RBC/gas ratios were significantly lower in IPF group than healthy volunteer group, the results indicated the possible application of monitoring and early diagnosis of IPF.

Asthma

Asthma is one of the most common respiratory conditions worldwide that leads to variable airway obstruction. Spirometry is a reliable tool used to monitor disease progression in clinical practice, but it can present with a false negative since asymptomatic patients with normal PFT can have airway inflammation (67), and it cannot provide regional airflow information within the lung. Previous studies indicated that hyperpolarized gas MRI offers a sensitive and noninvasive method to visualize airflow obstruction of the lung with the quantitative index of VDP. VDP is a biomarker in obstructive lung disease measured from HP gas MRI, depicting regional changes of airflow obstruction, and is associated with asthma severity and spirometry indices (17,68).

McIntosh et al conducted a retrospective study involving adults with asthma and healthy volunteers (69), HP ^{129}Xe MRI and spirometry were performed and the minimal clinically important difference and upper limit of normal for VDP were calculated in two groups. The results showed there was a moderate relationship in VDP between the two groups. The authors concluded that the minimal clinically important difference for asthma provides a way to interpret VDP measurements.

Pediatric asthma is likely to be a future development trend. The characteristics of pediatric asthma are less impaired lung function and persistent symptoms but higher exacerbation frequency (70,71). In a study of the pediatric population with asthma (72), spirometry results were collected, HP ^{129}Xe MRI was performed, and VDP based on the image was calculated, and the results showed that VDP is predictive of asthma outcomes, including asthma severity, healthcare utilization and oral corticosteroid use.

Cystic Fibrosis

Cystic fibrosis (CF) is a genetic disorder characterized by mucus accumulation, infection, inflammation and airway obstruction, several organs can be impacted by CF, but more than 80% of CF-related deaths are caused by lung morbidities (73). The lung clearance index (LCI), derived from the nitrogen multiple breath washout tests, is a commonly used clinical indicator of prognosis (74) and is more sensitive than the forced expiratory volume in 1 s (FEV_1) in detecting

ventilation inhomogeneity in early lesions, but LCI is a comprehensive score that does not provide spatial information (75). CT is currently the gold standard for the evaluation of structural changes in CF (76) but has certain limitations due to radiation exposure and unfavorable follow-up. VDP obtained from HP ^{129}Xe MRI is more sensitive than FEV_1 to minor lung changes (77–79) and can show regional redistribution of ventilation that cannot be obtained with PFT (80).

In a study of the application of HP ^{129}Xe MRI in cystic fibrosis, 11 patients ($\text{FEV}_1 > 70\%$) were recruited, Thomen et al hypothesized that ^{129}Xe MRI would demonstrate ventilation defects in mild CF lung disease (79), and the results showed that HP ^{129}Xe MRI is feasible in the detection of focal ventilation defects and is more sensitive than FEV_1 in detecting cystic fibrosis. In a similar research, Couch et al (78) assessed preserved lung function through the measurement of VDP and determined the relationship between FEV_1 and LCI, they concluded that there was a significant difference between VDP in CF patients and healthy volunteers, and mild-moderate negative correlation was shown between VDP and FEV_1 .

In a subsequent research, Couch et al (81) applied two imaging methods in pediatric CF populations including 6 patients with clinically stable CF and 11 patients undergoing a pulmonary exacerbation (PEX), the two methods were referred to as phase-resolved functional lung magnetic resonance imaging (PREFUL MRI, first introduced by Vogel Claussen group (82)) and HP ^{129}Xe MRI. The VDP obtained from the two imaging methods was separately calculated and compared, and the results showed that the stable CF group had a normal FEV_1 and an elevated LCI, while the PEX CF group had a reduced FEV_1 and an elevated LCI. Furthermore, VDPs obtained from HP ^{129}Xe MRI were correlated with that from PREFUL MRI, the mean VDP obtained from HP ^{129}Xe MRI in the PEX CF group was significantly greater than that in the healthy group. The above results indicated that HP ^{129}Xe MRI can quantify disease severity and detect early lesions through the VDP measurements, which may be helpful in early detection and treatment in clinical practice.

Pulmonary Hypertension

Pulmonary hypertension (PH) is a group of diseases that have long-term effects of multiple causes, leading to remodeling, hardening, stenosis, and occlusion of the pulmonary arteries, resulting in progressive elevation of pulmonary vascular resistance and pulmonary arterial pressure and ultimately leading to right heart failure (83,84), which affects pulmonary blood flow and alveolar gas exchange. The decrease in DL_{CO} is a common clinical manifestation of pulmonary vascular disease (85).

Virgincar et al established a rat model of pulmonary hypertension (86), and a normal control group was included in the research as well, both two groups underwent HP ^{129}Xe MRI. The results showed that ventilation was largely normal in the

PH group, with only a few animals presented with low ventilation; Barrier uptake manifested as normal or greater in the PH group compared to the control group and RBC transfer was decreased in the PH group; The RBC: barrier ratio was decreased, which is consistent with the results of Dahhan et al, for whom the RBC: barrier ratio was reported the first time to be reduced in PH and pulmonary veno-occlusive disease (87). The decreased RBC: barrier ratio was strongly correlated with DL_{CO} , the interstitial barrier thickness and reduced perfusion may be the cause of it. Wang et al performed HP ^{129}Xe MRI in 10 PH patients and found that there was a reduction in RBC transfer, slight elevation in ventilation and barrier uptake, and reduction in RBC transfer in PH patients (88). These findings suggest that HP ^{129}Xe MRI may be helpful in the diagnosis of PH, but further studies are required to determine its sensitivity and specificity.

Radiation-induced Lung Injury

Radiation therapy plays an important role in the treatment of lung cancer, the therapeutic dose is limited by radiation pneumonitis during the treatment, some patients will recover from the acute stage of radiation-induced lung injury, while some patients will develop clinically severe pulmonary fibrosis or irreversible chronic symptomatic stage of lung injury (89). Several studies have pointed out that radiation pneumonitis is better predicted when radiation treatment planning is correlated with lung function. Several groups have concluded that either a pulmonary perfusion or ventilation map is required to obtain functional information, and then incorporate it into the dose-volume analysis of the lungs to obtain dose-functional metrics that were more predictive of radiation pneumonitis (90–91). Although perfusion and ventilation are important cornerstones of the pulmonary system, it is gas exchange that ultimately determines lung function, several previous studies have demonstrated that HP ^{129}Xe MRI can quantify local exchange in the lungs (47,92–95).

In order to determine the correlation of lung ventilation and gas exchange and to discover the region of interest suited for radiation therapy, HP ^{129}Xe MRI was performed on three patients diagnosed with non-small cell lung cancer (NSCLC) in Rankine's study (96), maps in three states were obtained, including gaseous, dissolved interstitially and transferred to RBCs, and the results indicated that there was only a mild-moderate correlation between ventilation and gas exchange even in normal healthy volunteers. In a subsequent study, Rankine et al applied HP ^{129}Xe MRI for functional avoidance treatment planning in thoracic radiation therapy (97), treatment planning was further divided into ventilation-guided and gas-exchange guided treatments in this research, HP ^{129}Xe MRI were performed in 11 patients diagnosed with NSCLC before and after the treatment, and barrier uptake and RBC transfer was mapped separately; The results showed that gas-exchange treatment plan was more effective for regions of the lung with higher gas exchange to reduce mean lung dose.

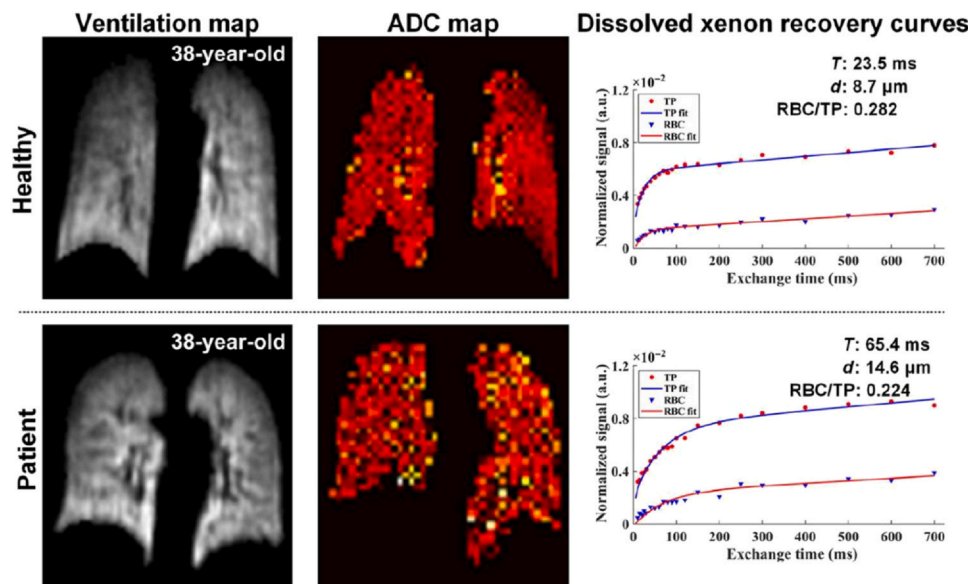


Figure 5. Ventilation maps, ADC maps, and dissolved Xe recovery curves are shown for a healthy subject and a discharged COVID-19 patient (103).

In a preliminary study of function-based radiation therapy planning for lung cancer using HP ^{129}Xe MRI (98), two radiation therapy plans were performed in ten advanced NSCLS patients, including anatomic plan(plan-A) based on CT alone and function-based plan(plan-F) based on both CT and MRI. The results showed that the $V_{5\text{Gy}}$, $V_{10\text{Gy}}$, $V_{20\text{Gy}}$ of high-functional lungs were significantly reduced in Plan-F, which indicated that HP ^{129}Xe MRI is expected to reduce radiation dose to lung tissue in areas of good ventilation function.

COVID-19

COVID-19 is an infectious disease caused by severe acute respiratory syndrome coronavirus 2 (SARS-CoV-2) (99). Some patients were reported to have persistent signs and symptoms, these patients are being given the diagnosis Long-COVID, post-acute COVID-19 syndrome (PACS), or post-acute sequelae of COVID-19 (PASC) (100), with Long-COVID being more commonly used. Long-COVID is a condition that involves multiple organs and presents with a range of symptoms, and it still is a research focus and remains difficult to manage patients with symptoms, despite being more than three years into the pandemic.

In a 1-year follow-up study involving patients with post-acute COVID-19 syndrome (101), HP ^{129}Xe MRI, PFT and St George Respiratory Questionnaire (SGRQ) were completed 3 months and 15 months after infection, and the results showed 34%(18 of 53) patients reported the VDP improvement and the mean VDP and SGRQ score both improved at the 15 months after infection. In a subsequent analysis, Kooner et al hypothesized that abnormal VDP in previous studies may derive from patients with prior respiratory disease (102); Therefore, they further divided

participants into subgroups with and without prior respiratory disease, the results showed that there was significantly improved VDP in the patients without lung disease while there were no significant improvements in patients with self-reported lung disease, and they concluded that patients with PACS without previous respiratory disease may be improved over time, but those with lung disease may be improved based on different timing.

Li et al evaluated pulmonary ventilation, gas exchange function, and microstructure changes caused by COVID-19 using HP ^{129}Xe MRI for the first time in 2020 (103). They found a slightly higher VDP in the COVID-19 patients (5.5%) than the healthy volunteers (3.7%) and unchanged microstructural parameters. Moreover, a longer gas exchange time constant was also found in the patients with COVID-19. These findings suggest that regional ventilation and alveolar airspace dimensions are relatively normal after discharge, while gas exchange function is diminished (Fig 5).

Grist et al evaluated the possible causes of breathlessness in patients with COVID-19 at 3 months after discharge using HP ^{129}Xe MRI and the results showed abnormalities of gas transfer in patients with post-COVID-19 pneumonia (104). In a subsequent study, HP ^{129}Xe MRI was used to identify gas transfer impairment in the lungs of nonhospitalized dyspneic participants with post-COVID-19 conditions and normal CT findings (105).

AI IN HYPERPOLARIZED GAS IMAGING

Clinical Applications

The application of artificial intelligence (AI) in pulmonary X-ray and CT is relatively extensive, while pulmonary MRI mainly focuses on AI-based lung MRI image segmentation

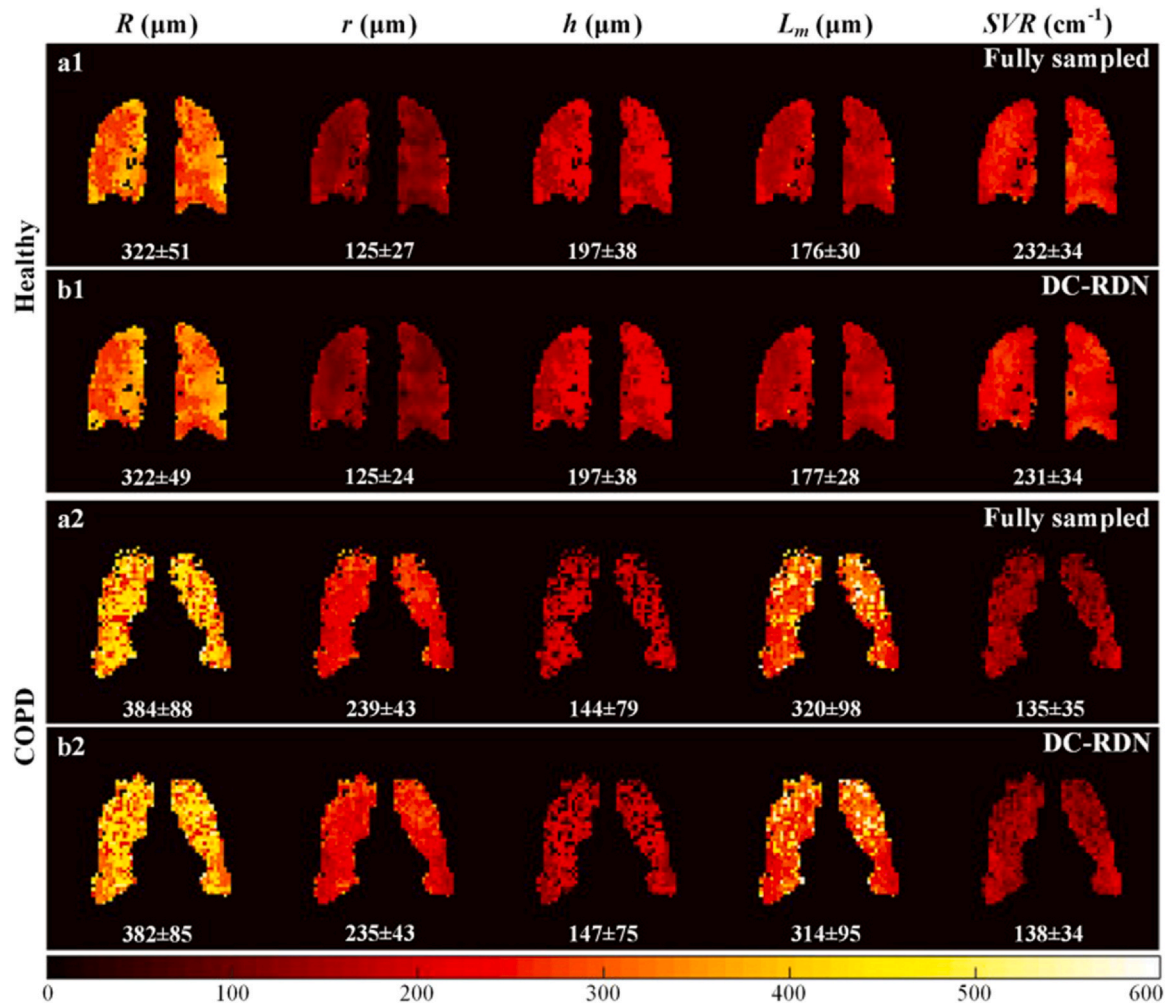


Figure 6. Lung morphometry maps derived from the DC-RDN reconstructed images at an acceleration factor of 4. DC-RDN was proposed by the team of Zhou Xin (106).

and reconstruction algorithm enhancement. Zhou's team first introduced deep learning (DL) into HP gas MRI and multiple b -value HP gas diffusion-weighted MRI (DW-MRI) reconstruction (32,106) (Fig 6). Astley et al also adopted DL approaches for ventilated lung segmentation using HP gas MRI and made a comparison between two conventional methods (spatial fuzzy c -means (SFCM) and K-means), and they indicated that DL approaches provide accurate and rapid segmentation of the lung, outperform two conventional segmentation methods (Fig 7) and exclude non-lung regions that may result in misunderstanding in subsequent analysis (107). The quality of images reconstructed with deep learning surpassed that of conventional methods, paving the way for future use of DL in real-time and accurate reconstruction of gas MRI.

Moreover, the segmentation domain of HP gas MRI has also witnessed the prowess of DL. Zhou and colleagues proposed a complementation-reinforced network of pulmonary gas MRI (called RS-Net) (108), as shown in Figure 8, for simultaneous reconstruction and segmentation of pulmonary gas MRI, enhancing the reconstruction and segmentation performance at

high acceleration factors up to 6. A hybrid DL configuration was proposed in HP gas MRI, which is capable of accurately replicating ventilation (109). Additionally, Astley et al developed a multimodal DL approach (110), integrating ^{129}Xe -MRI and ^1H -MRI, in a dual-channel convolutional neural network, and compared this approach to single-channel, taking lung cavity estimation as a benchmark, and further assessed VDP using DL-based framework and manually-based approach.

With the continuous evolution of AI algorithms and HP gas MRI, we could foresee a marked enhancement in imaging speed and segmentation precision of HP gas MRI, converging towards real-time acquisition and analysis. Such advances would not only enhance the patient experience by minimizing the time cost of the MRI scans but also enable clinicians to make swift decisions, especially in acute clinical scenarios. Beyond these realms, the potential of AI in HP gas MRI extends to predictive disease analytics and sophisticated denoising. For example, by harnessing the power of AI algorithms, it will become feasible to anticipate disease progression trends and outcomes based solely on initial HP gas MRI scans. Such insights can offer a forecast into disease

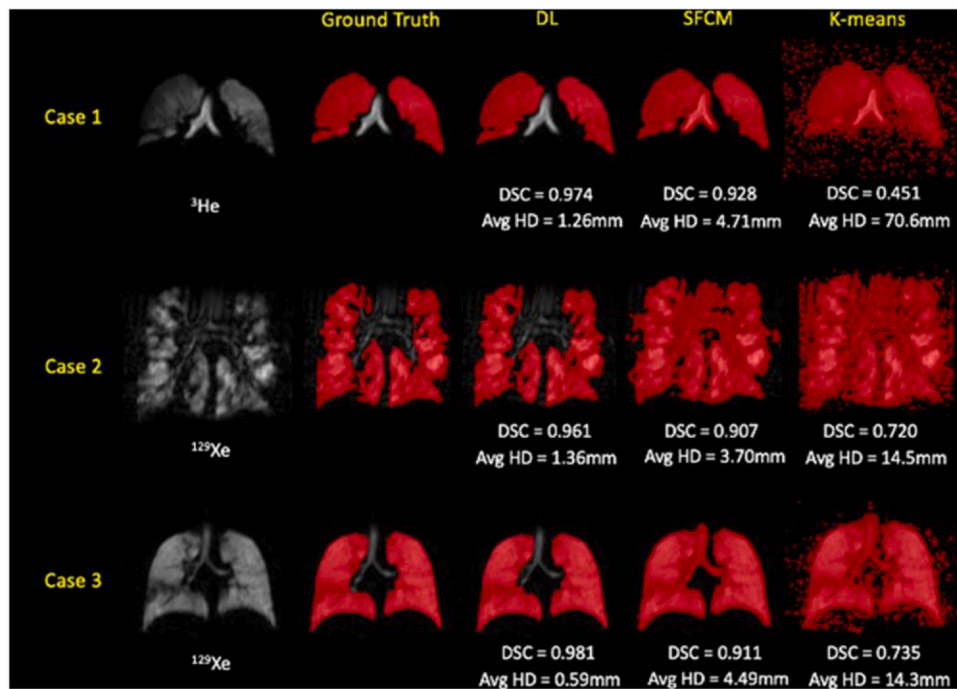


Figure 7. Comparison of performance on testing scans between DL method and conventional methods (SFCM and K-means) (107).

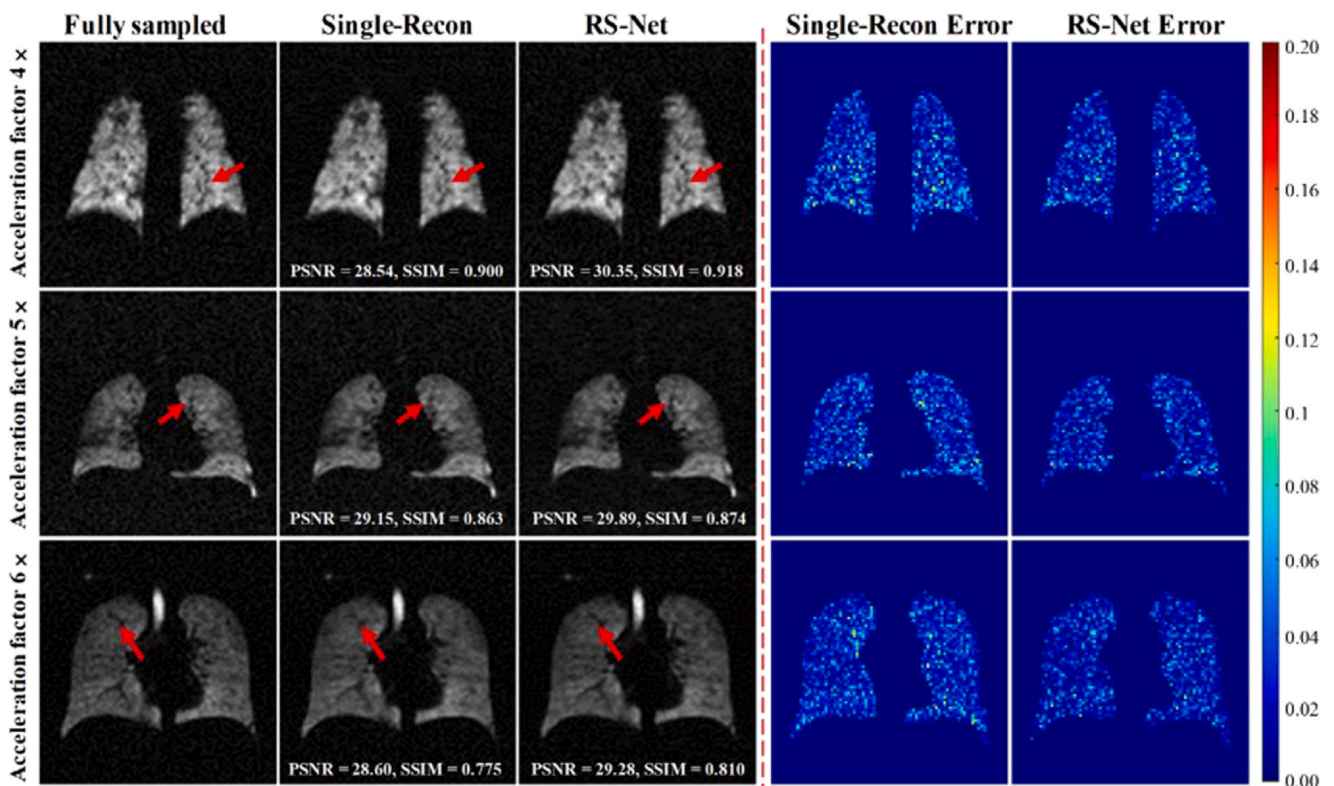


Figure 8. Reconstructed hyperpolarized gas MR images obtained by RS-Net proposed by the team of Zhou with an acceleration factor of 4, 5, 6 (108).

progression, allowing medical professionals to preemptively strategize treatment regimens, potentially improving patient outcomes. AI-driven denoising techniques are emerging as

potent tools for reducing background noise. Sophisticated denoising algorithms can extract the essential information from HP gas MRI while simultaneously suppressing unwanted artifacts.

This enhancement in image fidelity promises not only improved diagnostic accuracy but also the potential discovery of subtle pathologies previously masked by noise. In conclusion, as AI and HP gas MRI increasingly intertwine, their combination will offer significant benefits for clinical practice.

Future Perspectives of DL in HP ^{129}Xe MRI

Due to the significant advantages of DL in exerting big data, large computing power, improving the performance of reconstruction, segmentation, and other algorithms, and speeding up the operation speed, DL will be continuously applied to HP ^{129}Xe MRI in the future. However, its application will also be limited by its lack of interpretability (black box), high requirements for the accuracy of data labels, and significant performance degradation across platforms and centers. With the development of AI, such as chatgpt-4 and others, maybe these limitations will be solved well.

CLINICAL APPLICATIONS OF HP ^{129}Xe MRI

There are some challenges in the clinical application of hyperpolarized ^{129}Xe MRI. First, specialized equipment was required for the hyperpolarization of the gas, which was named the polarizer. With the development of technology, commercial polarizers have matured. Second, a radiofrequency coil and MRI with multinuclear capabilities for image acquisition were also needed. Third, image analysis algorithms and software for image analysis and data processing were significant. At present, a set of effective and modular image analysis processes and algorithms have been formed in this field, so the complexity of data analysis can be better solved for clinical application. Fourth, highly trained technical staff for the hyperpolarized ^{129}Xe MRI was also necessary. However, the gradual maturity of image analysis and processing software will gradually reduce the professional requirements for this group of people. Finally, the economic and logistical challenges of the clinical application of hyperpolarized ^{129}Xe MRI cannot be ignored, including the upgrade of a clinical MRI scanner, required hardware and software, gas costs, routine maintenance, and upgrade, and so on. With the development of technology, hyperpolarized ^{129}Xe MRI shows great potential in clinical application for all the challenges.

CONCLUSION

Hyperpolarized ^{129}Xe MRI is a promising MRI technology that emerged in the last two decades, which can obtain structural and functional images of the lungs through dynamic spectroscopy, 3D imaging and other techniques, and has unique advantages for the dynamic observation of lung diseases, especially in the application of lung diseases such as COPD, IPF, and CF. Ventilation, barrier uptake and RBC transfer can be assessed respectively, showing better diagnostic efficacy than some clinical indicators, which has great potential for subsequent clinical work. Currently, clinical use of ^{129}Xe was first approved in 2020 by the

National Medical Products Administration (NMPA) and in 2022 by the FDA, and the MRI scanner that could image ^{129}Xe was approved by NMPA in August 2023. Although hyperpolarized ^{129}Xe MRI is a high sensitivity, safe, non-ionizing method for lung imaging, it has some limitations, from a practical perspective, there remains a need for the standardization of imaging procedure (including polarization equipment installation, personnel training, standardized scanning protocol and post-processed techniques), the relatively expensive fee compared to other clinical examinations may be the major consideration in the further translation to clinical practice, and multi-center prospective randomized clinical trials are required to obtain more clinical data to promote the development and further clinical application of the MRI technique.

FUNDING STATEMENT

This work was supported by the National Natural Science Foundation of China (grant numbers: 82171926, 81930049); National Key R&D Program of China (grant number: 2022YFC2010000, 2022YFC2010002, 2022YFC2010005).

DECLARATION OF COMPETING INTEREST

The authors declare that they have no known competing financial interests or personal relationships that could have appeared to influence the work reported in this paper.

REFERENCES

1. Dawood YT, Cook NE, Graham WB, et al. Smoking-associated interstitial lung disease: update and review. *Expert Rev Respir Med* 2020; 14(8):825–834.
2. Evans-Polce R, Veliz P, et al. Trends in e-cigarette, cigarette, cigar, and smokeless tobacco use among US adolescent cohorts, 2014–2018. *Am J Public Health* 2020; 110(2):163–165.
3. Sverzellati N, Molinari F, Pirroni T, et al. New insights on COPD imaging via CT and MRI. *Int J Chron Obstruct Pulmon Dis* 2007; 2(3):301–312.
4. Roach PJ, Schembri GP, Bailey DL. V/Q scanning using SPECT and SPECT/CT. *J Nucl Med* 2013; 54(9):1588–1596.
5. Swift AJ, Wild JM, Nagle SK, et al. Quantitative magnetic resonance imaging of pulmonary hypertension: a practical approach to the current state of the art. *J Thorac Imaging* 2014; 29(2):68–79.
6. Liang J, Li J, Li Z, et al. Differentiating the lung lesions using Intravoxel incoherent motion diffusion-weighted imaging: a meta-analysis. *BMC Cancer* 2020; 20(1):799. Published 2020 Aug 24.
7. Johns CS, Swift AJ, Rajaram S, et al. Lung perfusion: MRI vs. SPECT for screening in suspected chronic thromboembolic pulmonary hypertension. *J Magn Reson Imaging* 2017; 46(6):1693–1697.
8. Benlala I, Berger P, Girodet PO, et al. Automated volumetric quantification of emphysema severity by using ultrashort echo time MRI: validation in participants with chronic obstructive pulmonary disease. *Radiology* 2019; 292(1):216–225.
9. Ohno Y, Nishio M, Koyama H, et al. Pulmonary MR imaging with ultrashort TEs: utility for disease severity assessment of connective tissue disease patients. *Eur J Radiol* 2013; 82(8):1359–1365.
10. Weiger M, Wu M, Wumig MC, et al. Rapid and robust pulmonary proton ZTE imaging in the mouse. *NMR Biomed* 2014; 27(9):1129–1134.
11. Bianchi A, Tibiletti M, Kjørstad Å, et al. Three-dimensional accurate detection of lung emphysema in rats using ultra-short and zero echo time MRI. *NMR Biomed* 2015; 28(11):1471–1479.
12. de Lange EE, Mugler 3rd JP, Brookeman JR, et al. Lung air spaces: MR imaging evaluation with hyperpolarized ^3He gas. *Radiology* 1999; 210(3):851–857.

13. Patz S, Muradian I, Hrovat MI, et al. Human pulmonary imaging and spectroscopy with hyperpolarized ^{129}Xe at 0.2T. *Acad Radiol* 2008; 15(6):713–727.
14. van Beek EJ, Dahmen AM, Stavngaard T, et al. Hyperpolarised ^3He MRI versus HRCT in COPD and normal volunteers: PHIL trial. *Eur Respir J* 2009; 34(6):1311–1321.
15. Stavngaard T, Sogaard LV, Mortensen J, et al. Hyperpolarized ^3He MRI and ^81mKr SPECT in chronic obstructive pulmonary disease. *Eur J Nucl Med Mol Imaging* 2005; 32(4):448–457.
16. Altes TA, Powers PL, Knight-Scott J, et al. Hyperpolarized ^3He MR lung ventilation imaging in asthmatics: preliminary findings. *J Magn Reson Imaging* 2001; 13(3):378–384.
17. de Lange EE, Altes TA, Patrie JT, et al. Evaluation of asthma with hyperpolarized helium-3 MRI: correlation with clinical severity and spirometry. *Chest* 2006; 130(4):1055–1062.
18. Mentore K, Froh DK, de Lange EE, et al. Hyperpolarized ^3He MRI of the lung in cystic fibrosis: assessment at baseline and after bronchodilator and airway clearance treatment. *Acad Radiol* 2005; 12(11):1423–1429.
19. Kirby M, Svenningsen S, Ahmed H, et al. Quantitative evaluation of hyperpolarized helium-3 magnetic resonance imaging of lung function variability in cystic fibrosis. *Acad Radiol* 2011; 18(8):1006–1013.
20. Mathew L, Gaede S, Wheatley A, et al. Detection of longitudinal lung structural and functional changes after diagnosis of radiation-induced lung injury using hyperpolarized ^3He magnetic resonance imaging. *Med Phys* 2010; 37(1):22–31.
21. Kirby M, Svenningsen S, Owringi A, et al. Hyperpolarized ^3He and ^{129}Xe MR imaging in healthy volunteers and patients with chronic obstructive pulmonary disease. *Radiology* 2012; 265(2):600–610.
22. Peiffer JD, Altes T, Russet IC, et al. Hyperpolarized ^{129}Xe MRI, $^{99\text{m}}\text{Tc}$ scintigraphy, and SPECT in lung ventilation imaging: a quantitative comparison. Published online November 15. *Acad Radiol* 2023. Published online November 15.
23. Barskiy DA, Coffey AM, Nikolau P, et al. NMR hyperpolarization techniques of gases. *Chemistry* 2017; 23(4):725–751.
24. Zhou X. Hyperpolarized noble gases as contrast agents. *Methods Mol Biol* 2011; 771:189–204.
25. Zeng Q, Bie B, Guo Q, et al. Hyperpolarized Xe NMR signal advancement by metal-organic framework entrapment in aqueous solution. *Proc Natl Acad Sci U S A* 2020; 117(30):17558–17563.
26. Horn FC, Rao M, Stewart NJ, et al. Multiple breath washout of hyperpolarized ^{129}Xe and ^3He in human lungs with three-dimensional balanced steady-state free-precession imaging. *Magn Reson Med* 2017; 77(6):2288–2295.
27. Zhong J, Ruan W, Han Y, et al. Fast determination of flip angle and T_1 in hyperpolarized gas MRI during a single breath-hold. *Sci Rep* 2016; 6:25854. Published 2016 May 12.
28. He M, Driehuys B, Que LG, et al. Using hyperpolarized ^{129}Xe MRI to quantify the pulmonary ventilation distribution. *Acad Radiol* 2016; 23(12):1521–1531.
29. Mummy DG, Kruger SJ, Zha W, et al. Ventilation defect percent in helium-3 magnetic resonance imaging as a biomarker of severe outcomes in asthma. *J Allergy Clin Immunol* 2018; 141(3):1140–1141.e4.
30. Marshall H, Deppe MH, Parra-Robles J, et al. Direct visualisation of collateral ventilation in COPD with hyperpolarised gas MRI. *Thorax* 2012; 67(7):613–617.
31. Doganay O, Wade T, Hegarty E, McKenzie C, Schulte RF, Santyr GE. Hyperpolarized (^{129}Xe) Xe imaging of the rat lung using spiral IDEAL. *Magn Reson Med* 2016; 76(2):566–576.
32. Duan C, Deng H, Xiao S, et al. Fast and accurate reconstruction of human lung gas MRI with deep learning. *Magn Reson Med* 2019; 82(6):2273–2285.
33. Ajraoui S, Lee KJ, Deppe MH, et al. Compressed sensing in hyperpolarized ^3He lung MRI. *Magn Reson Med* 2010; 63(4):1059–1069.
34. Xiao S, Deng H, Duan C, et al. Highly and adaptively undersampling pattern for pulmonary hyperpolarized ^{129}Xe dynamic MRI. *IEEE Trans Med Imaging* 2019; 38(5):1240–1250.
35. Xiao S, Deng H, Duan C, et al. Considering low-rank, sparse and gas-inflow effects constraints for accelerated pulmonary dynamic hyperpolarized ^{129}Xe MRI. *J Magn Reson* 2018; 290:29–37.
36. Chan HF, Collier GJ, Parra-Robles J, et al. Finite element simulations of hyperpolarized gas DWI in micro-CT meshes of acinar airways: validating the cylinder and stretched exponential models of lung microstructural length scales. *Magn Reson Med* 2021; 86(1):514–525.
37. Zhang H, Xie J, Xiao S, et al. Lung morphometry using hyperpolarized ^{129}Xe multi-b diffusion MRI with compressed sensing in healthy subjects and patients with COPD. *Med Phys* 2018; 45(7):3097–3108.
38. Zhou Q, Li H, Rao Q, et al. Assessment of pulmonary morphometry using hyperpolarized ^{129}Xe diffusion-weighted MRI with variable-sampling-ratio compressed sensing patterns. *Med Phys* 2023; 50(2):867–878.
39. Bdaoui AS, Niedbalski PJ, Hossain MM, et al. Improving hyperpolarized ^{129}Xe ADC mapping in pediatric and adult lungs with uncertainty propagation. *NMR Biomed* 2022; 35(3):e4639.
40. Thomen RP, Quirk JD, Roach D, et al. Direct comparison of ^{129}Xe diffusion measurements with quantitative histology in human lungs. *Magn Reson Med* 2017; 77(1):265–272.
41. Saunders LC, Collier GJ, Chan HF, et al. Longitudinal lung function assessment of patients hospitalized With COVID-19 using ^1H and ^{129}Xe lung MRI. *Chest* 2023; 164(3):700–716.
42. Chan HF, Weatherley ND, Johns CS, et al. Airway microstructure in idiopathic pulmonary fibrosis: assessment at hyperpolarized ^3He diffusion-weighted MRI. *Radiology* 2019; 291(1):223–229.
43. Tafti S, Garrison WJ, Mugler 3rd JP, et al. Emphysema index based on hyperpolarized ^3He or ^{129}Xe diffusion MRI: performance and comparison with quantitative CT and pulmonary function tests. *Radiology* 2020; 297(1):201–210.
44. Stewart NJ, Leung G, Norquay G, et al. Experimental validation of the hyperpolarized ^{129}Xe chemical shift saturation recovery technique in healthy volunteers and subjects with interstitial lung disease. *Magn Reson Med* 2015; 74(1):196–207.
45. Chang YV. MOXE: a model of gas exchange for hyperpolarized ^{129}Xe magnetic resonance of the lung. *Magn Reson Med* 2013; 69(3):884–890.
46. Patz S, Muradian I, Hrovat MI, et al. Diffusion of hyperpolarized ^{129}Xe in the lung: a simplified model of ^{129}Xe septal uptake and experimental results [J]. *New J Phys* 2011; 13(1):015009.
47. Kaushik SS, Robertson SH, Freeman MS, et al. Single-breath clinical imaging of hyperpolarized (^{129}Xe) in the airspaces, barrier, and red blood cells using an interleaved 3D radial 1-point Dixon acquisition. *Magn Reson Med* 2016; 75(4):1434–1443.
48. Niedbalski PJ, Lu J, Hall CS, et al. Utilizing flip angle/TR equivalence to reduce breath hold duration in hyperpolarized ^{129}Xe 1-point Dixon gas exchange imaging. *Magn Reson Med* 2022; 87(3):1490–1499.
49. Qing K, Mugler 3rd JP, Altes TA, et al. Assessment of lung function in asthma and COPD using hyperpolarized ^{129}Xe chemical shift saturation recovery spectroscopy and dissolved-phase MRI. *NMR Biomed* 2014; 27(12):1490–1501.
50. Kammerman J, Hahn AD, Cadman RV, et al. Transverse relaxation rates of pulmonary dissolved-phase hyperpolarized ^{129}Xe as a biomarker of lung injury in idiopathic pulmonary fibrosis. *Magn Reson Med* 2020; 84(4):1857–1867.
51. Collier G.J., Eaden J.A., Hughes P.J.C., et al. Dissolved ^{129}Xe lung MRI with four-echo 3D radialspectroscopic imaging: Quantification of regional gas transfer in idiopathic pulmonary fibrosis. *Magn Reson Med*.
52. Xie J, Li H, Zhang H, et al. Single breath-hold measurement of pulmonary gas exchange and diffusion in humans with hyperpolarized ^{129}Xe MR. *NMR Biomed* 2019; 32(5):e4068.
53. Mummy DG, Coleman EM, Wang Z, et al. Regional gas exchange measured by ^{129}Xe magnetic resonance imaging before and after combination bronchodilators treatment in chronic obstructive pulmonary disease. *J Magn Reson Imaging* 2021; 54(3):964–974.
54. Wang Z, Robertson SH, Wang J, et al. Quantitative analysis of hyperpolarized ^{129}Xe gas transfer MRI. *Med Phys* 2017; 44(6):2415–2428.
55. Chen M, Doganay O, Matin T, et al. Delayed ventilation assessment using fast dynamic hyperpolarized Xenon-129 magnetic resonance imaging. *Eur Radiol* 2020; 30(2):1145–1155.
56. Matin TN, Rahman N, Nickol AH, et al. Chronic obstructive pulmonary disease: lobar analysis with hyperpolarized ^{129}Xe MR Imaging. *Radiology* 2017; 282(3):857–868.
57. Qing K, Tustison NJ, Mugler 3rd JP, et al. Probing changes in lung physiology in COPD using CT, perfusion MRI, and hyperpolarized xenon-129 MRI. *Acad Radiol* 2019; 26(3):326–334.
58. Doganay O, Matin T, Chen M, et al. Time-series hyperpolarized xenon-129 MRI of lobar lung ventilation of COPD in comparison to V/Q-SPECT/CT and CT. *Eur Radiol* 2019; 29(8):4058–4067.

59. American Thoracic Society. Idiopathic pulmonary fibrosis: diagnosis and treatment. International consensus statement. American Thoracic Society (ATS), and the European Respiratory Society (ERS). *Am J Respir Crit Care Med* 2000; 161(2 Pt 1):646–664.
60. Plantier L, Cazes A, Dinh-Xuan AT, et al. Physiology of the lung in idiopathic pulmonary fibrosis. *Eur Respir Rev* 2018; 27(147):170062. Published 2018 Jan 24.
61. Raghu G, Remy-Jardin M, Myers JL, et al. Diagnosis of idiopathic pulmonary fibrosis. An official ATS/ERS/JRS/ALAT clinical practice guideline. *Am J Respir Crit Care Med* 2018; 198(5):e44–e68.
62. Mura M, Ferretti A, Ferro O, et al. Functional predictors of exertional dyspnea, 6-min walking distance and HRCT fibrosis score in idiopathic pulmonary fibrosis. *Respiration* 2006; 73(4):495–502.
63. Mammarrappallil JG, Rankine L, Wild JM, et al. New developments in imaging idiopathic pulmonary fibrosis with hyperpolarized xenon magnetic resonance imaging. *J Thorac Imaging* 2019; 34(2):136–150.
64. Kaushik SS, Freeman MS, Yoon SW, et al. Measuring diffusion limitation with a perfusion-limited gas–hyperpolarized ^{129}Xe gas-transfer spectroscopy in patients with idiopathic pulmonary fibrosis. *J Appl Physiol* (1985) 2014; 117(6):577–585.
65. Wang JM, Robertson SH, Wang Z, et al. Using hyperpolarized ^{129}Xe MRI to quantify regional gas transfer in idiopathic pulmonary fibrosis. *Thorax* 2018; 73(1):21–28.
66. Hahn AD, Carey KJ, Barton GP, et al. Hyperpolarized ^{129}Xe MR spectroscopy in the lung shows 1-year reduced function in idiopathic pulmonary fibrosis. *Radiology* 2022; 305(3):688–696.
67. Kavuru MS, Dweik RA, Thomassen MJ. Role of bronchoscopy in asthma research. *Clin Chest Med* 1999; 20(1):153–189.
68. Zha W, Kruger SJ, Cadman RV, et al. Regional heterogeneity of lobar ventilation in asthma using hyperpolarized helium-3 MRI. *Acad Radiol* 2018; 25(2):169–178.
69. McIntosh MJ, Biancianiello A, Kooner HK, et al. ^{129}Xe MRI ventilation defects in asthma: what is the upper limit of normal and minimal clinically important difference? Published online April 7 *Acad Radiol* 2023. Published online April 7.
70. Jenkins HA, Cherniack R, Szefer SJ, et al. A comparison of the clinical characteristics of children and adults with severe asthma. *Chest* 2003; 124(4):1318–1324.
71. Trivedi M, Denton E. Asthma in children and adults—what are the differences and what can they tell us about asthma? *Front Pediatr* 2019; 7:256. Published 2019 Jun 25.
72. Lin NY, Roach DJ, Willmerring MM, et al. ^{129}Xe MRI as a measure of clinical disease severity for pediatric asthma. *J Allergy Clin Immunol* 2021; 147(6):2146–2153.e1.
73. Shteinberg M, Haq IJ, Polineni D, et al. Cystic fibrosis. *Lancet* 2021; 397(10290):2195–2211.
74. Aurora P, Bush A, Gustafsson P, et al. Multiple-breath washout as a marker of lung disease in preschool children with cystic fibrosis. *Am J Respir Crit Care Med* 2005; 171(3):249–256.
75. Stanojevic S, Jensen R, Sundaralingam D, et al. Alternative outcomes for the multiple breath washout in children with CF. *J Cyst Fibros* 2015; 14(4):490–496.
76. de Jong PA, Ottink MD, Robben SG, et al. Pulmonary disease assessment in cystic fibrosis: comparison of CT scoring systems and value of bronchial and arterial dimension measurements. *Radiology* 2004; 231(2):434–439.
77. Couch MJ, Morgado F, Kanhere N, et al. Assessing the feasibility of hyperpolarized ^{129}Xe multiple-breath washout MRI in pediatric cystic fibrosis. *Magn Reson Med* 2020; 84(1):304–311.
78. Couch MJ, Thomen R, Kanhere N, et al. A two-center analysis of hyperpolarized ^{129}Xe lung MRI in stable pediatric cystic fibrosis: potential as a biomarker for multi-site trials. *J Cyst Fibros* 2019; 18(5):728–733.
79. Thomen RP, Walkup LL, Roach DJ, et al. Hyperpolarized ^{129}Xe for investigation of mild cystic fibrosis lung disease in pediatric patients. *J Cyst Fibros* 2017; 16(2):275–282.
80. Rayment JH, Couch MJ, McDonald N, et al. Hyperpolarised ^{129}Xe magnetic resonance imaging to monitor treatment response in children with cystic fibrosis. *Eur Respir J* 2019; 53(5):1802188. Published 2019 May 2.
81. Couch MJ, Munidasa S, Rayment JH, et al. Comparison of functional free-breathing pulmonary ^1H and hyperpolarized ^{129}Xe magnetic resonance imaging in pediatric cystic fibrosis. *Acad Radiol*. 2021; 28(8):e209–e218.
82. Voskrebenezov A, Gutberlet M, Klimeš F, et al. Feasibility of quantitative regional ventilation and perfusion mapping with phase-resolved functional lung (PREFUL) MRI in healthy volunteers and COPD, CTEPH, and CF patients. *Magn Reson Med* 2018; 79(4):2306–2314.
83. Schannwell CM, Steiner S, Strauer BE. Diagnostics in pulmonary hypertension. *J Physiol Pharmacol* 2007; 58 Suppl 5(Pt 2):591–602.
84. Chan SY, Loscalzo J. Pathogenic mechanisms of pulmonary arterial hypertension. *J Mol Cell Cardiol* 2008; 44(1):14–30.
85. Farha S, Laskowski D, George D, et al. Loss of alveolar membrane diffusing capacity and pulmonary capillary blood volume in pulmonary arterial hypertension. *Respir Res* 2013; 14(1):6. Published 2013 Jan 22.
86. Virgincar RS, Nouis JC, Wang Z, et al. Quantitative ^{129}Xe MRI detects early impairment of gas-exchange in a rat model of pulmonary hypertension. *Sci Rep* 2020; 10(1):7385. Published 2020 Apr 30.
87. Dahhan T, Kaushik SS, He M, et al. Abnormalities in hyperpolarized (^{129}Xe) magnetic resonance imaging and spectroscopy in two patients with pulmonary vascular disease. *Pulm Circ* 2016; 6(1):126–131.
88. Wang Z, Bier EA, Swaminathan A, et al. Diverse cardiopulmonary diseases are associated with distinct xenon magnetic resonance imaging signatures. *Eur Respir J* 2019; 54(6):1900831. Published 2019 Dec 12.
89. Tsoutsou PG, Koukourakis MI. Radiation pneumonitis and fibrosis: mechanisms underlying its pathogenesis and implications for future research. *Int J Radiat Oncol Biol Phys* 2006; 66(5):1281–1293.
90. Farr KP, Kallehauge JF, Møller DS, et al. Inclusion of functional information from perfusion SPECT improves predictive value of dose-volume parameters in lung toxicity outcome after radiotherapy for non-small cell lung cancer: a prospective study. *Radiother Oncol* 2015; 117(1):9–16.
91. Vinogradskiy Y, Castillo R, Castillo E, et al. Use of 4-dimensional computed tomography-based ventilation imaging to correlate lung dose and function with clinical outcomes. *Int J Radiat Oncol Biol Phys* 2013; 86(2):366–371.
92. Hahn AD, Kammerman J, Evans M, et al. Repeatability of regional pulmonary functional metrics of Hyperpolarized ^{129}Xe dissolved-phase MRI. *J Magn Reson Imaging* 2019; 50(4):1182–1190.
93. Mugler 3rd JP, Altes TA, Ruset IC, et al. Simultaneous magnetic resonance imaging of ventilation distribution and gas uptake in the human lung using hyperpolarized xenon-129. *Proc Natl Acad Sci U S A* 2010; 107(50):21707–21712.
94. Qing K, Ruppert K, Jiang Y, et al. Regional mapping of gas uptake by blood and tissue in the human lung using hyperpolarized xenon-129 MRI. *J Magn Reson Imaging* 2014; 39(2):346–359.
95. Driehuys B, Cofer GP, Pollaro J, et al. Imaging alveolar-capillary gas transfer using hyperpolarized ^{129}Xe MRI. *Proc Natl Acad Sci U S A* 2006; 103(48):18278–18283.
96. Rankine LJ, Wang Z, Driehuys B, et al. Correlation of regional lung ventilation and gas transfer to red blood cells: implications for functional-avoidance radiation therapy planning. *Int J Radiat Oncol Biol Phys* 2018; 101(5):1113–1122.
97. Rankine LJ, Wang Z, Kelsey CR, et al. Hyperpolarized ^{129}Xe magnetic resonance imaging for functional avoidance treatment planning in thoracic radiation therapy: a comparison of ventilation- and gas exchange-guided treatment plans. *Int J Radiat Oncol Biol Phys* 2021; 111(4):1044–1057.
98. Ding Y, Yang L, Zhou Q, et al. A pilot study of function-based radiation therapy planning for lung cancer using hyperpolarized xenon-129 ventilation MRI. *J Appl Clin Med Phys* 2022; 23(3):e13502.
99. Zhou F, Yu T, Du R, et al. Clinical course and risk factors for mortality of adult inpatients with COVID-19 in Wuhan, China: a retrospective cohort study [published correction appears in *Lancet*. 2020 Mar 28;395(10229):1038] [published correction appears in *Lancet*. 2020 Mar 28;395(10229):1038]. *Lancet* 2020; 395(10229):1054–1062.
100. Proal AD, VanElzakker MB. Long COVID or post-acute sequelae of COVID-19 (PASC): an overview of biological factors that may contribute to persistent symptoms. *Front Microbiol* 2021; 12:698169. Published 2021 Jun 23.
101. Kooner HK, McIntosh MJ, Matheson AM, et al. Postacute COVID-19 syndrome: ^{129}Xe MRI ventilation defects and respiratory outcomes 1 year later. *Radiology* 2023; 307(2):e222557.
102. Kooner HK, McIntosh MJ, Matheson AM, et al. More data about ^{129}Xe MRI ventilation defects in long COVID-19. *Radiology* 2023; 307(4):e230479.

103. Li H, Zhao X, Wang Y, et al. Damaged lung gas exchange function of discharged COVID-19 patients detected by hyperpolarized ^{129}Xe MRI. *Sci Adv* 2021; 7(1):eabc8180. Published 2021 Jan 1.
104. Grist JT, Chen M, Collier GJ, et al. Hyperpolarized ^{129}Xe MRI abnormalities in dyspneic patients 3 months after COVID-19 pneumonia: preliminary results. *Radiology* 2021; 301(1):E353–E360.
105. Grist JT, Collier GJ, Walters H, et al. Lung abnormalities detected with hyperpolarized ^{129}Xe MRI in patients with long COVID. *Radiology* 2022; 305(3):709–717.
106. Duan C, Deng H, Xiao S, et al. Accelerate gas diffusion-weighted MRI for lung morphometry with deep learning. *Eur Radiol* 2022; 32(1):702–713.
107. Astley JR, Biancardi AM, Hughes PJC, et al. Large-scale investigation of deep learning approaches for ventilated lung segmentation using multi-nuclear hyperpolarized gas MRI. *Sci Rep* 2022; 12(1):10566. Published 2022 Jun 22.
108. Li Z, Xiao S, Wang C, et al. Complementation-reinforced network for integrated reconstruction and segmentation of pulmonary gas MRI with high acceleration [published online ahead of print, 2023 Jul 3]. *Med Phys* 2023. <https://doi.org/10.1002/mp.16591>
109. Astley JR, Biancardi AM, Marshall H, et al. A hybrid model- and deep learning-based framework for functional lung image synthesis from multi-inflation CT and hyperpolarized gas MRI. *Med Phys* 2023; 50(9):5657–5670.
110. Astley JR, Biancardi AM, Marshall H, et al. A dual-channel deep learning approach for lung cavity estimation from hyperpolarized gas and proton MRI. *J Magn Reson Imaging* 2023; 57(6):1878–1890.